# Single-Site Cobalt Catalysts at New $Zr_8(\mu_2\text{-O})_8(\mu_2\text{-OH})_4$ Metal-Organic Framework Nodes for Highly Active Hydrogenation of Alkenes, Imines, Carbonyls, and Heterocycles

Pengfei Ji,[†] Kuntal Manna,[†] Zekai Lin, Ania Urban, Francis X. Greene, Guangxu Lan, and Wenbin Lin[*]

Department of Chemistry, University of Chicago, 929 E. 57th St., Chicago, Illinois 60637, United States

Ⓢ Supporting Information

ABSTRACT: We report here the synthesis of robust and porous metal−organic frameworks (MOFs), M-MTBC (M = Zr or Hf), constructed from the tetrahedral linker methane-tetrakis (*p*-biphenylcarboxylate) (MTBC) and two types of secondary building units (SBUs): cubic $M_8(\mu_2\text{-O})_8(\mu_2\text{-OH})_4$ and octahedral $M_6(\mu_3\text{-O})_4(\mu_3\text{-OH})_4$. While the M_6-SBU is isostructural with the 12-connected octahedral SBUs of UiO-type MOFs, the M_8-SBU is composed of eight M^{IV} ions in a cubic fashion linked by eight μ_2-oxo and four μ_2-OH groups. The metalation of Zr-MTBC SBUs with $CoCl_2$, followed by treatment with $NaBEt_3H$, afforded highly active and reusable solid Zr-MTBC-CoH catalysts for the hydrogenation of alkenes, imines, carbonyls, and heterocycles. Zr-MTBC-CoH was impressively tolerant of a range of functional groups and displayed high activity in the hydrogenation of tri- and tetra-substituted alkenes with TON > 8000 for the hydrogenation of 2,3-dimethyl-2-butene. Our structural and spectroscopic studies show that site isolation of and open environments around the cobalt-hydride catalytic species at Zr_8-SBUs are responsible for high catalytic activity in the hydrogenation of a wide range of challenging substrates. MOFs thus provide a novel platform for discovering and studying new single-site base-metal solid catalysts with enormous potential for sustainable chemical synthesis.
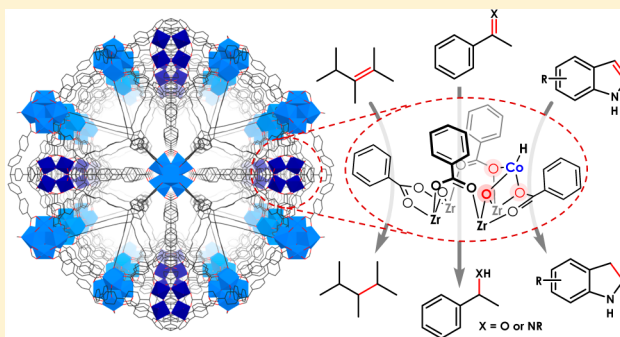
INTRODUCTION

Hydrogenation of unsaturated organic compounds is one of the most widely practiced metal-catalyzed reactions in organic synthesis and the chemical industry, with applications in the production of commodity chemicals, pharmaceuticals, and agrochemicals.[1] For decades, hydrogenation reactions have relied on precious metal catalysts supported either on solid surfaces[2] or by strong field ligands[3] to enable two-electron redox chemistry—oxidative addition and reductive elimination—that constitute key bond-breaking and bond-forming steps in the catalytic cycle. However, the low abundance, high price, and inherent toxicity of precious metals have led to intense interest in developing earth-abundant metal catalysts.[4] Significant progress has been made in recent years on the development of single-site hydrogenation catalysts based on iron, cobalt, nickel, or copper coordinated with sterically encumbered strong field nitrogen- or phosphorus-donor ligands.[5] However, each homogeneous base metal catalyst typically only hydrogenates a narrow class of substrates with limited turnover numbers. Furthermore, few examples of earth-abundant metal-catalyzed hydrogenation of imines and heterocycles exist, and all of them require harsh reaction conditions.[6]

Homogeneous base metal catalysts typically rely on coordination of sterically bulky chelating ligands to prevent the formation of catalytically incompetent oligomeric species by shutting down the intermolecular decomposition pathways.

Such steric protection is important for stabilizing weak-field ligand-coordinated metal catalysts, particularly for late first-row transition metals in a very weak field coordination environment consisting of oxygen-donor atoms.[7] However, steric protecting groups often weaken metal−ligand binding and impede the catalytic activity by preventing challenging hydrogenation substrates, such as tri- and tetra- substituted olefins, from accessing the catalytic sites.[8] Immobilization of catalytic species in structurally regular porous solid supports can provide catalytic site isolation without relying on bulky ligands, thus offering an alternative route to obtaining highly active base metal catalysts. Significant efforts have been devoted to the development of zeolite-, silica-, or graphene-supported iron- and cobalt-based heterogeneous hydrogenation catalysts[6a,9] and bare or protected metallic nanoparticles-based catalysts.[10] However, the activities and stability of these heterogeneous hydrogenation catalysts are still far from satisfactory.

Metal−organic frameworks (MOFs),[11] constructed from metal cluster secondary building units (SBUs) and organic linkers, have emerged as a tunable class of porous and crystalline supports for discovering reusable single-site solid catalysts for organic transformations.[12] By using premetalated organic struts or via postsynthetic metalation of functionalized bridging linkers,

MOFs have provided a highly tunable platform to engineer single-site solid catalysts for many organic transformations that cannot be performed by traditional porous inorganic materials.[13] Furthermore, the SBUs of MOFs consisting of inorganic oxide clusters can be used as oxygen-donor ligands,[14] thus providing an unprecedented opportunity for developing robust, site-isolated, base-metal catalysts in a weak field coordination environment. The synthetic tunability of MOFs makes it possible to fine-tune electronic and steric properties of catalytic active sites, whereas the structure regularity and site homogeneity of MOFs greatly facilitate mechanistic studies of MOF-catalyzed reactions.

We recently designed a highly active and chemoselective cobalt-hydride catalyst supported on the $Zr_6(\mu_3\text{-O})_4(\mu_3\text{-OH})_4$ node of UiO-68 MOF for benzylic C−H functionalization and olefin hydrogenation.[15] Although the potential of Zr_3-μ_3-OH as a ligand site was realized, the μ_3-OH site is surrounded by three phenyl rings around 105° apart from each other, which forms a very sterically encumbered local environment, thus making the Zr_3-μ_4-O-CoH catalyst inactive in the hydrogenation of challenging substrates, such as tetrasubstituted olefins and heterocycles. Design and synthesis of analogous Zr-based clusters with open environments around the SBUs would make the metal node-supported cobalt catalysts more active in the hydrogenation of challenging substrates and thus potentially applicable in industrial hydrogenations. Here we report a new $Zr_8(\mu_2\text{-O})_8(\mu_2\text{-OH})_4$ MOF node with sterically open Zr_2-μ_2-OH ligand sites that

support Co-based catalysts for the hydrogenation of a broad range of unsaturated compounds such as olefins, imines, carbonyls, and heterocycles.

RESULTS AND DISCUSSION

Synthesis of M-MTBC (M = Zr or Hf) MOFs. Zr-MTBC was synthesized in 54% yield via a solvothermal reaction between $ZrCl_4$ and $4',4''',4''''',4'''''''$-methanetetrayltetrakis([1,1'-biphenyl]-4-carboxylic acid) (H_4MTBC) in DEF using benzoic acid as modulator. A single-crystal X-ray diffraction study of Zr-MTBC indicated that Zr-MTBC crystallizes in the cubic $pm3n$ space group and revealed the presence of two types of SBUs, $Zr_8(\mu_2\text{-O})_8(\mu_2\text{-OH})_4$ and the $Zr_6(\mu_3\text{-O})_4(\mu_3\text{-OH})_4$ in 1:3 ratio (Figure 1a). To our knowledge, the $Zr_8(\mu_2\text{-O})_8(\mu_2\text{-OH})_4$ SBU has not been synthesized before as either a discrete cluster or as a structural unit in a MOF.[16] In the $Zr_8(\mu_2\text{-O})_8(\mu_2\text{-OH})_4$ SBU, eight Zr^{IV} ions occupy the eight corners of the cube, while eight μ_2-oxo and four μ_2-OH occupy the 12 edges of the cube. The $Zr_6(\mu_3\text{-O})_4(\mu_3\text{-OH})_4$ unit is isostructural to the SBU of UiO-MOF, with six Zr^{IV} ions occupying six corners of an octahedron that are held together by four μ_3-oxo and four μ_3-OH groups at eight faces of the octahedron. Solid-state infrared spectrum (IR) spectrum showed the presence of both the $\nu_{\mu_2\text{O−H}}$ stretching band at 3737 cm^{-1} and $\nu_{\mu_3\text{O−H}}$ stretching band at 3639 cm^{-1} (Figure 1b). The void space was calculated to be 73.53% by PLATON. The MOF possessed two kinds of trigonal-bipyramid cavities
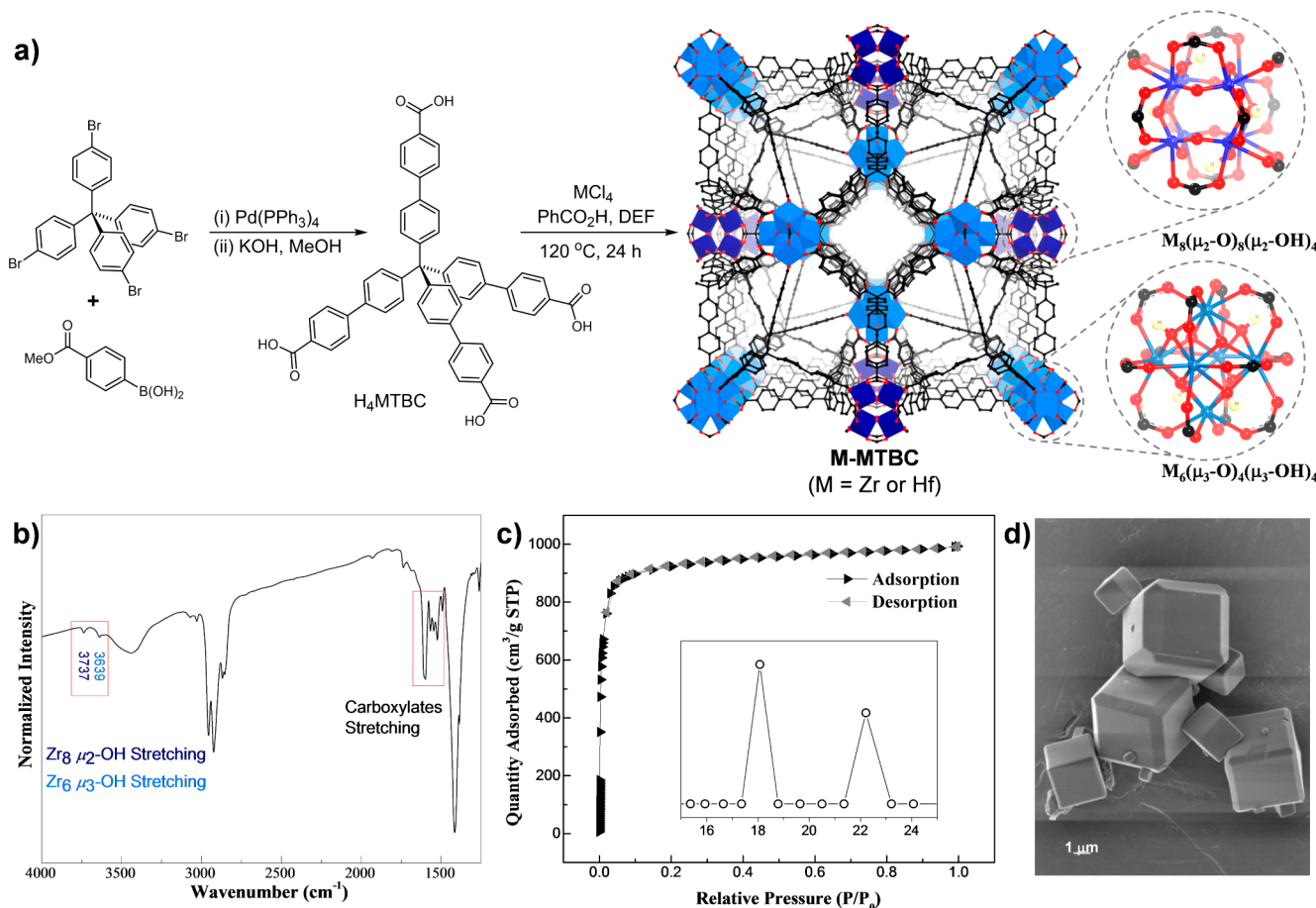

Figure 1. (a) The synthesis of M-MTBC (M = Zr or Hf). (b) IR spectrum of Zr-MTBC showing stretching vibration of μ_3-OH at 3639 cm^{-1} from Zr_6-SBU and μ_2-OH at 3737 cm^{-1} from Zr_8-SBU. (c) Nitrogen sorption isotherms of Zr-MTBC (77 K). Inset shows pore size distribution in Å. (d) SEM image of Zr-MTBC.

of dimensions 24.9 × 21.6 × 35.9 Å and 20.8 × 20.8 × 13.1 Å, respectively. N_2 adsorption isotherm of Zr-MTBC showed a type I adsorption (77 K, 1 bar) with Brunauer–Emmett–Teller (BET) surface area of 3700 m^2/g (Figure 1c). SEM and TEM images showed cubic particles of 1–3 μm in length (Figure 1d). The Hf-MTBC analog was synthesized similarly and characterized by single-crystal X-ray diffraction (Figure S9, SI).

Metalation of Zr-MTBC with CoCl₂. Zr-MTBC was treated with 10 equiv of ^{n}BuLi to deprotonate both the μ_2-OH's in Zr_8-SBU and the μ_3-OH's in Zr_6-SBU, then reacted with a $CoCl_2$ solution in THF to afford Zr-MTBC-CoCl as a deep-blue solid (Figure 2a).

Both the carboxylate groups and the linkers remained intact during lithiation and metalation, as evidenced by a ^{1}H NMR spectrum of the digested Zr-MTBC-CoCl in D_3PO_4/DMSO-d_6 (Figure S15, SI) and by the retention of strong carboxylate carbonyl stretching in the IR spectrum (Figure 1b). The disappearance of both the ν_{μ_2O-H} band (3737 cm^{-1}) and ν_{μ_3O-H} band (3639 cm^{-1}) in the IR spectrum indicated that the metalation occurred at both SBU sites (Figure S12, SI). Inductively coupled plasma-mass spectrometry (ICP-MS) analysis of the digested MOF revealed complete metalation of all Zr_8 and Zr_6 clusters, corresponding to four Co centers per Zr_8 or Zr_6 node. Crystallinity of the MOF was maintained after metalation, as indicated by the similarity between the powder X-ray diffraction (PXRD) patterns of Zr-MTBC and Zr-MTBC-CoCl (Figure 2b). However, the coordination environments of the Co centers in Zr-MTBC-CoCl could not be established by X-ray diffraction due to intrinsic disorder of coordinated cobalt atoms (Figure S16, SI), similar to our previously reported examples.[15] We instead used X-ray adsorption spectroscopy (XAS) to investigate Co coordination environments. Four out of six faces of the $Zr_8(\mu_2$-O$)_8(\mu_2$-OH$)_4$ cubic node had a μ_2-OH group that could be lithiated and used for Co binding (Figure 2a). We envisioned two different Co coordination modes on the Zr_8 node: μ_2-oxide/μ_2-oxo chelation and μ_2-oxide/(μ-carboxylate)$_2$ tridentate binding. We realized that the μ_2-oxide/μ_2-oxo chelation binding mode would not be ideal because the μ_2-oxide to μ_2-oxo distance was only 2.35 Å, too short for chelation to the same Co center. Such a structural model does not fit the extended X-ray adsorption fine structure (EXAFS) data (Figure S19, SI). In contrast, the μ_2-oxide and two μ-carboxylate groups could coordinate to the same Co center in a stable conformation, with Co to μ_2-oxide distance of 1.88 Å and Co to μ-carboxylate distance of 2.00 Å, as indicated by the EXAFS fitting result (Figure 2d). Cobalt coordination on Zr_6 node also adopts a μ_2-oxide/(μ-carboxylate)$_2$ tridentate mode, identical to that observed in the previously studied UiO-68-CoCl system.[15]

Activation of Zr-MTBC-CoCl with NaBEt₃H for Olefin Hydrogenation. Treating Zr-MTBC-CoCl with 5 equiv of $NaBEt_3H$ in THF generated the cobalt-hydride species Zr-MTBC-CoH as a black solid. We did not observe the formation of hydrogen gas by GC analysis, indicating H/Cl metathesis during the activation step. The reaction of Zr-MTBC-CoH with 10 equiv of formic acid at room temperature or with excess water at 75 °C readily generated an equivalent amount of H_2 (Figure S21, SI),[17] supporting the identity of Zr-MTBC-CoH. XANES analysis of Zr-MTBC-CoH suggested a +2 oxidation state of Co (Figure 2c). EXAFS fitting on Zr-MTBC-CoH indicated that the Co adopts μ_2-oxide/(μ-carboxylate)$_2$ tridentate binding mode, with Co to μ_2-oxide distance of 1.83 Å and Co to η_2-carboxylate distance of 1.94, similar to the structure proposed for Zr-MTBC-CoCl (Figure 2e).

Zr-MTBC-CoH proved to be a highly active catalyst for hydrogenation of a range of alkenes in THF at room temperature. At a 0.05 mol % Co loading, terminal alkenes containing oxo-, carboxy-, pyridyl-, or silyl-functionalities—allyl ether, allyl acetate, dimethyl itaconate, 2-vinylpyridine, and allyltrimethylsilane—were selectively hydrogenated to afford dipropylether, propylacetate, dimethyl 2-methylsuccinate, 2-ethylpyridine, and propyltrimethylsilane, respectively, in quantitative yields (entries 1–6, Table 1). At a 0.05–0.1 mol % Co loading, Zr-MTBC-CoH was also very active in hydrogenation of trisubstituted alkenes such as ethyl-3,3- dimethyl acrylate, α-terpinene, trans-α-methyl-stilbene, and 1-methyl-1-cyclohexene, and corresponding pure hydrogenated products were obtained in excellent yields by simple filtration of reaction mixtures followed by removal of the volatiles (entries 8–12, Table 1). Impressively, Zr-MTBC-CoH completely hydrogenated tetrasubstituted alkenes such as 2,3-dimethyl-2-butene at room temperature within 48 h to afford 2,3-dimethylbutane with a TON > 8000 (entry 13, Table 1). Hydrogenation of bulkier tetrasubstituted alkenes such as 2,3,4-trimethylpent-2-ene could also be achieved at elevated temperatures, which facilitated their diffusion through MOF channels as well as the binding and activation of the substrate at the cobalt-site (entry 14, Table 1). It has been previously observed that $Zr_3(\mu_4$-O)Co site in Zr_6-SBU of UiO-68 is inactive in catalyzing the hydrogenation of bulky and rigid trisubstituted alkenes such as 1-methyl-1-cyclohexene and tetrasubstituted alkenes.[15] Therefore, we believe that the hydrogenation of these bulky alkenes occurred exclusively at the $Zr_2(\mu_3$-O)Co sites in Zr_8-SBUs of Zr-MTBC-CoH. The hydrogenation of 6-methyl-5-hepten-2-one to 6-methyl-2-heptanone catalyzed by Pd/C or Pd/Al₂O₃ is a key step to synthesizing dimethyloctenol (DMOE), an important fragrance compound.[18] At a 0.5 mol % Co loading, Zr-MTBC-CoH also selectively hydrogenated 6-methyl-5-hepten-2-one at 40 °C to afford 6-methyl-2-heptanone in quantitative yield (entry 15, Table 1). Interestingly, 6-methyl-2-heptanol was obtained quantitatively upon heating the reaction mixture at 80 °C (entry 16, Table 1).

Importantly, at a 0.1 mol % Co-loading, Zr-MTBC-CoH could be recovered and reused at least 5 times for the hydrogenation of 1-methylcyclohexene (Figure 3) without loss of MOF crystallinity (Figure 2b). Excellent yields (92–100%) of methylcyclohexane were obtained consistently in the reuse experiments with no observation of other byproducts (Figure S25, SI). The PXRD patterns of Zr-MTBC-CoH recovered from the first and sixth runs remained unchanged from that of pristine Zr-MTBC-CoH (Figure 2b), indicating the stability of the MOF under reaction conditions. The heterogeneity of Zr-MTBC-CoH was confirmed by several experiments. ICP-MS analyses showed that the amounts of Co and Zr that leached into the supernatant after the first run were only 1.6% and 0.02%, respectively. Moreover, the rate of hydrogenation was unchanged in the presence of mercury, and no additional hydrogenation was observed after removal of Zr-MTBC-CoH from the reaction mixture, which ruled out the role of the leached Co-nanoparticles or other Co-species in catalyzing hydrogenation reactions (Figure S24, SI).

Mechanistic Investigation of Zr-MTBC-CoH-Catalyzed Hydrogenation of 1-Methylcyclohexene. As discussed above, the treatment of Zr-MTBC-CoCl with $NaEt_3BH$ in THF generated Zr-MTBC-CoH species, which is likely the active catalyst in the hydrogenation reactions. The EXAFS spectrum of Zr-MTBC-Co recovered from hydrogenation of 1-methylcyclohexene showed the absence of Co–Co scattering from Co nanoparticles, ruling out the formation of any Co-nanoparticles
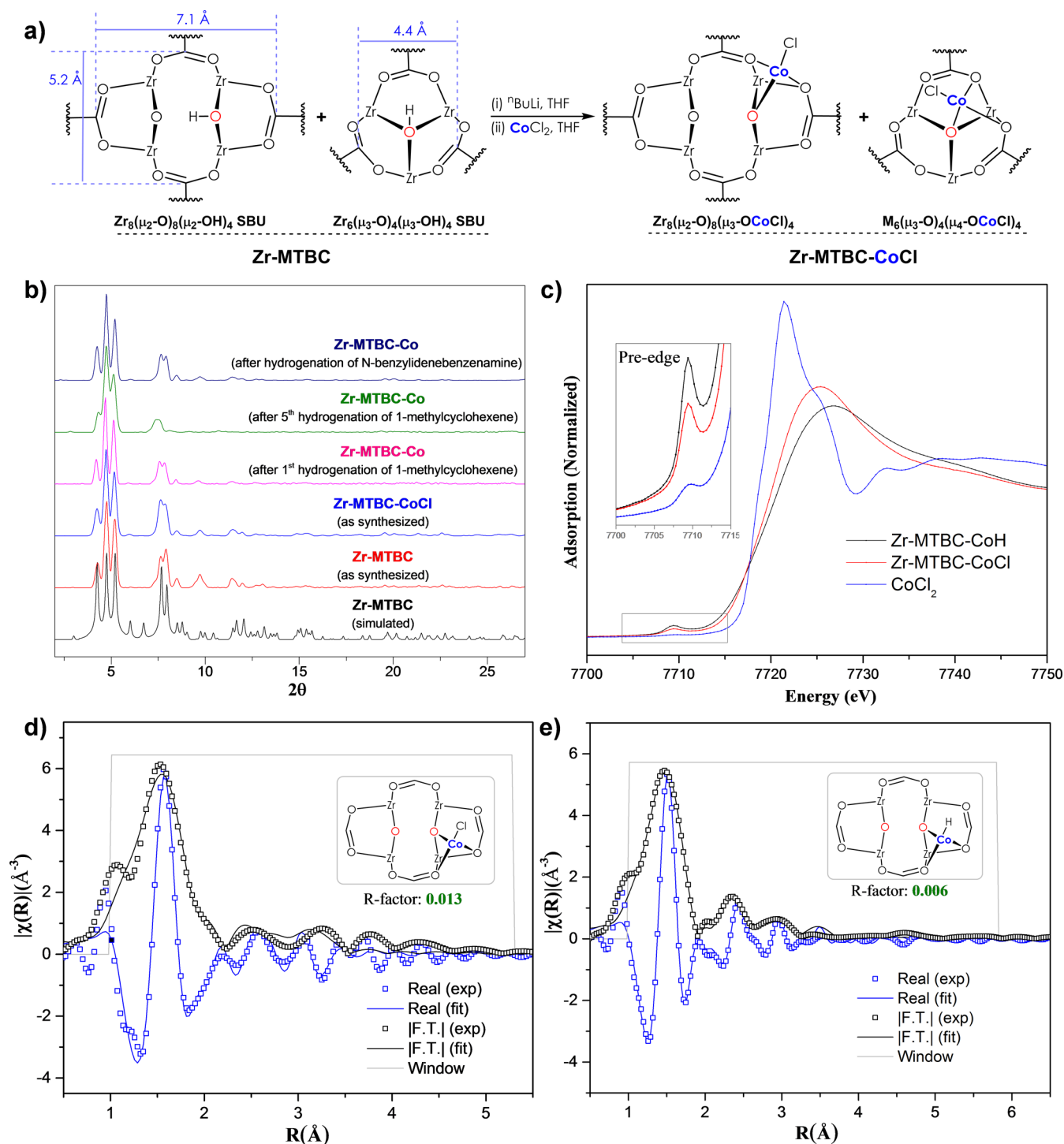
Figure 2. (a) The metalation of Zr$_8$-SBUs and Zr$_6$-SBUs of Zr-MTBC with CoCl$_2$ to form Zr-MTBC-CoCl. (b) Similarities among the PXRD patterns simulated from the CIF file of Zr-MTBC (black) and the PXRD patterns of as-synthesized Zr-MTBC (red), Zr-MTBC-CoCl (blue), Zr-MTBC-CoH samples recovered from hydrogenation of 1-methylcyclohexene after runs 1 (pink) and 6 (green) and after hydrogenation of *N*-benzylidenebenzenamine (navy) show the retention of Zr-MTBC crystallinity after metalation and catalysis. (c) XANES spectra of Zr-MTBC-CoCl and Zr-MTBC-CoH are similar to that of CoCl$_2$, indicating a +2 oxidation state for the Co centers in Zr-MTBC-CoCl and Zr-MTBC-CoH. (d) EXAFS spectra and fits in R-space at the Co K-edge of Zr-MTBC-CoCl showing the magnitude (hollow squares, black) and real component (hollow squares, blue) of the Fourier transformation. The fitting range is 1.2−5.6 Å in R space (within the gray lines). (e) EXAFS spectra and fits in R-space at the Co K-edge of Zr-MTBC-CoH showing the magnitude (hollow squares, black) and real component (hollow squares, blue) of the Fourier transformation. The fitting range is 1.2−5.8 Å in R space (within the gray lines).

during the catalysis (Figure S22, SI). To further investigate the mechanism, the rate law was determined by the method of initial rates (<15% conversion) in THF at room temperature. In order to avoid complications caused by the presence of two kinds of

Co-centers in Zr-MTBC-CoH, the initial rates were measured for hydrogenation of 1-methylcyclohexene catalyzed by only Zr$_2$(μ_3-O)Co sites, since Zr$_3$(μ_4-O)CoH at the SBUs of UiO-68 was inactive in hydrogenation of 1-methylcyclohexene. The empirical

Table 1. Zr-MTBC-CoH-Catalyzed Hydrogenation of Alkenes[a]

Entry	Substrate	Product	mol% Co	Time	Yield[b]	TON
1			0.05	1.5 d	100 (86)	>2000
2			0.05	1.5 d	100	>2000
3			0.05	1.5 d	100	>2000
4			0.2	1.5 d	100	>500
5			0.05	1.5 d	100 (99)	>2000
6			0.05	1.5 d	100	>2000
7			0.05	1.5 d	100 (99)	>2000
8			0.1	2 d	81	810
9			0.05	2 d	100 (91)	>2000
10[c]			0.05	2 d	100 dr; 1.3:1	>2000
11			0.05	1.5 d	100 (95)	>2000
12			0.05	12 h	100	>8000[d]
13			0.05	2 d	100	>8000[d]
14[c]			0.5	2 d	46	368[d]
15[e]			0.5	18 h	100	>200
16[f]			0.5	2 d	100	>200

[a]Reaction conditions: 0.25 mg of Zr-MTBC-CoCl, 5 equiv of NaBEt₃H (1.0 M in THF) w.r.t. Co, alkene, THF, 40 bar H₂, 23 °C. [b]Yields were determined by ¹H NMR with mesitylene as the internal standard. Isolated yield in the parentheses. [c]Reaction was performed at 70 °C in toluene. [d]TON was calculated based on only Zr₂(μ_3-O)Co sites. [e]Reaction was performed at 40 °C. [f]Reaction was performed at 80 °C in toluene.

rate law showed that the initial rates had a first-order dependence on the cobalt concentrations and P_{H_2} (Figure 4a) and a zeroth-order dependence on the alkene concentration (Figures 4a and S26, SI). The activation of H₂ at the electron-deficient Co(II)-center via oxidative addition is unlikely. Our kinetic and spectroscopic data thus suggest that the insertion of the C═C bond of the alkene into the Co−H bond generates a Co-alkyl intermediate, which undergoes σ-bond metathesis with H₂ in the turnover limiting step to give an alkane product, simultaneously regenerating the cobalt-hydride species (Figure 4b).

Zr-MTBC-CoH-Catalyzed Hydrogenation of Imines and Carbonyls. Prompted by the hydrogenation of the carbonyl group of 6-methyl-5-hepten-2-one at elevated temperatures, we

sought to investigate the hydrogenation of imines and carbonyls. Zr-MTBC-CoH also displayed excellent activity in catalytic hydrogenation of imines (Table 2). Though hydrogenation of imines is an important synthetic route to amines, examples of base metal catalysts for imine hydrogenation are rare.[6b] Our imine hydrogenation reactions were performed in toluene at 80 °C under 40 bar of H₂ in the presence of 0.5 mol % Zr-MTBC-CoH. N-benzylidenebenzenamine was completely hydrogenated to N-benzylaniline in 5 h. The pure product was isolated in 98% yield after simple filtration followed by removal of the volatiles in vacuo (entry 1, Table 1). The Zr-MTBC-CoH recovered after this reaction remained crystalline, as shown by PXRD (Figure 2b), and the leaching of Co and Zr into the supernatant was 0.23%
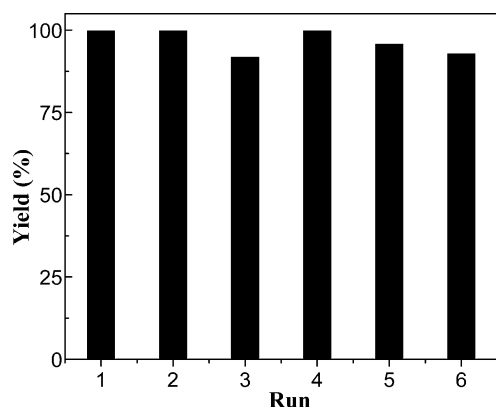
Figure 3. Plots of yields (%) of methylcyclohexane at different runs in the reuse experiments of Zr-MTBC-Co for hydrogenation of 1-methyl-cyclohexene. The Co loadings were ~0.1 mol %.
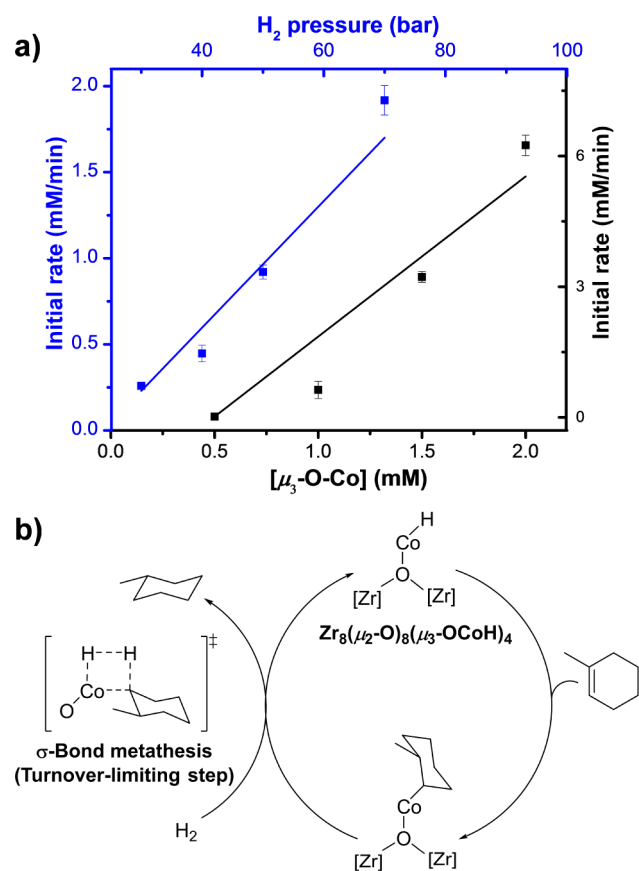

Figure 4. (a) Kinetic plots of initial rates (d[methylcyclohexane]/d*t*) for hydrogenation of 1-methylcyclohexene versus concentration of $Zr_2(\mu_3\text{-O})$ Co and hydrogen pressure for the first 35 min, showing first-order dependence on both components. (b) Proposed catalytic cycle: the insertion of the alkene into the Co–H bond gives a Co-alkyl species, followed by turnover limiting σ-bond metathesis with H_2 to generate the alkane product.

and 0.08%, respectively. *N*-(4-chlorobenzylidene)benzenamine, *N*-(2-methoxybenzylidene)benzenamine, *N*-(4-methoxy-benzylidene)benzenamine, and *N*-benzylidenebenzylamine were efficiently reduced within 24 h to afford corresponding *N*-benzylanilines in excellent yields (entries 2–5, Table 2). The hydrogenation of trisubstituted imines, such as (*E*)-*N*-(1-phenylethylidene)aniline, however, required longer reaction times (entry 7, Table 2), presumably due to the decreased rates

Table 2. Zr-MTBC-CoH-Catalyzed Hydrogenation of Imines[a]
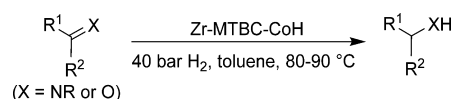
Entry	Substrate	Time	% Yield[b]
1		5 h	100 (98)
2		24 h	100
3		24 h	100 (90)
4		24 h	100 (99)
5		24 h	100
6		48 h	70
7		48 h	100
8		48 h	79
9		48 h	64
10		72 h	76
11		48 h	90

[a]Reaction conditions: 0.25 mg of Zr-MTBC-CoCl (0.5 mol % Co), 5 equiv of NaBEt$_3$H (1.0 M in THF) w.r.t. Co, alkene, toluene, 40 bar H_2, 80 °C. [b]Yields were determined by ^{1}H NMR with mesitylene as the internal standard. Isolated yield in the parentheses.

of diffusion of the larger substrate and product through the MOF channels and less facile binding and activation of the substrate.
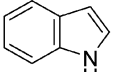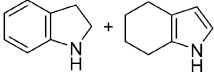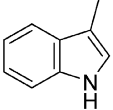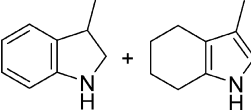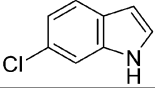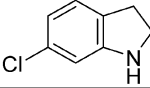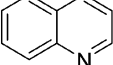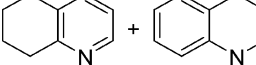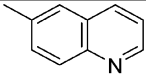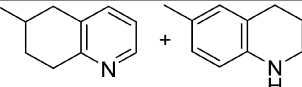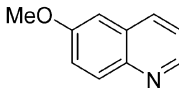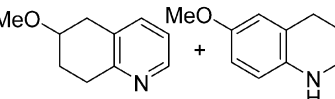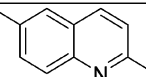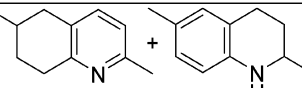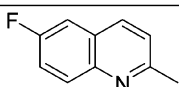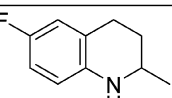
Zr-MTBC-CoH is also active in catalyzing hydrogenation of carbonyls to their corresponding alcohols in toluene at 90 °C.[5b,19] At a 0.5 mol % Co loading, Zr-MTBC-CoH afforded 1-phenylethanol, 1-(4-chlorophenyl)ethanol, and cyclohexanol from corresponding ketone substrates in good yields (entries 8–10, Table 1). Benzaldehyde was also efficiently reduced to benzyl alcohol in 90% isolated yield.

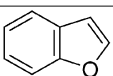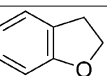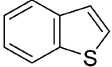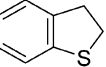**Zr-MTBC-CoH-Catalyzed Hydrogenation of Heterocycles.** The hydrogenation of heterocycles is challenging due to their resonance stabilization and potential poisoning of catalysts by substrates and their products. Although significant progress has been made in developing precious metal-based molecular and heterogeneous catalysts for selective hydrogenation of *N*-heteoarenes such as indoles and quinolines, the advancement of the analogous earth abundant-metal catalysts has lagged behind.[6a,20] Catalytic hydrogenation of *O*-heteroarenes such as furans and benzofurans is also significantly under-developed. Additionally, the hydrogenation of heteroarenes typically requires harsh reaction conditions, high catalyst loadings, and excess additives.

At a 0.5 mol % Co loading, Zr-MTBC-CoH-catalyzed hydrogenation of indole in toluene at 80 °C to affords a mixture of indoline and 4,5,6,7-tetrahydroindole. Indoline was obtained in 84% isolated yield after preparative thin-layer chromatography (entry 1, Table 3). Interestingly, hydrogenation of 3-methyl-indole gave 3-methyl-indoline and 3-methyl-4,5,6,7-tetrahydroindole in 46:54 ratio, which indicates that reduction of

the phenyl ring is also possible. Hydrogenation of quinolines in toluene at 80 °C gave a mixture of two products, 1,2,3,4-tetrahydroquinoline and 5,6,7,8-tetrahydro-quinoline in a 1:1 ratio. Under identical reaction conditions, the selectivity is highly dependent on the substitution of the phenyl ring. Electron-donating substituents at the 6-position of the quinolines favor the hydrogenation of phenyl ring. For example, the 6-methylquinoline, 6-methoxyquinoline, and 2,6-dimethylquinoline were hydrogenated to give 6-methyl-5,6,7,8-tetrahydro-quinoline, 6-methoxy-5,6,7,8-tetrahydro-quinoline, and 2,6-dimethyl-5,6,7,8-tetrahydro-quinoline, respectively, as the major products (entries 5−7, Table 3). In contrast, strong electron-withdrawing substituents disfavor the reduction of the phenyl ring. The hydrogenation of 2-methyl-6-fluoro-quinoline afforded 2-methyl-6-fluoro-1,2,3,4,-tetrahydro-quinoline exclusively in 72% yield (entry 8, Table 3). Interestingly, Zr-MTBC-CoH was also a very active catalyst for hydrogenation of benzofuran. At a 0.2 mol % Co loading, benzofuran was completely hydrogenated to 2,3-dihydrobenzofuran in qualitative yield (entry 9, Table 3).

Table 3. Zr-MTBC-CoH-Catalyzed Hydrogenation of Heterocycles[a]

Entry	Substrate	Product	Mol% Co	Time	Yield[b]
1			0.5	66 h	84 (93:7)
2[c]			0.5	72 h	87 (46:54)
3			0.5	72 h	16[d]
4			0.5	48 h	95 (50:50)
5			0.5	48 h	100 (60:40)
6			0.5	48 h	82 (74:26)
7			0.2	48 h	100 (84:16)
8			0.2	48 h	72
9			0.2	8 h	100
10			0.2	48 h	0

[a]Reaction conditions: 0.25 mg of Zr-MTBC-CoCl, 5 equiv of NaBEt$_3$H (1.0 M in THF) w.r.t. Co, alkene, toluene (2 mL), 40 bar H$_2$, 80 °C. [b]Yields were determined by ^{1}H NMR with mesitylene as the internal standard. Ratios of the products, as determined by GC-MS, are in the parentheses. [c]Reaction was performed at 100 °C. [d]Yields determined by GC-MS analysis.

CONCLUSION

We have synthesized new Zr- and Hf-based mixed-node MOFs with previously unknown $M_8(\mu_2\text{-}O)_8(\mu_2\text{-}OH)_4$ SBUs. As a result of active site isolation of and open environments of metal node-supported cobalt-hydride species, the cobalt-functionalized MOF was highly active in catalyzing hydrogenation of a broad scope of substrates, including highly hindered and unactivated alkenes, imines, carbonyls, and heterocycles. The high stability, low cost, and exceptional activity of metal node-supported MOF catalysts make them promising candidates for industrial application in the synthesis of commodity chemicals, phamaceuticals, and agrochemicals. Our simple yet powerful strategy of metalating MOF SBUs with readily available base-metal precursors could be used for the discovery of new uniformly distributed single-site catalysts with unprecedented activity and selectivity.

ASSOCIATED CONTENT

ⓈSupporting Information

The Supporting Information is available free of charge on the ACS Publications website at DOI: 10.1021/jacs.6b06759.

> Synthesis and characterization of the H_4MTBC ligand, Zr-MTBC and Zr-MTBC-CoCl, procedures for catalytic hydrogenation of alkenes, heterocycles and imines, details for X-ray absorption spectroscopic analysis, crystal structure figures and crystallographic files of Zr-MTBC, Hf-MTBC, and Zr-MTBC-CoCl. Crystallographic data can be obtained free of charge from The Cambridge Crystallographic Data Centre via www.ccdc.cam.ac.uk/data_request/cif
> (PDF)

Crystallographic data of Zr-MTBC (CCDC 1487038) (CIF)

Crystallographic data of Hf-MTBC (CCDC 1486780) (CIF)

Crystallographic data of Zr-MTBC-CoCl (CCDC 1486878) (CIF)

AUTHOR INFORMATION

Corresponding Author

*wenbinlin@uchicago.edu

Author Contributions

[†]These authors contributed equally.

Notes

The authors declare no competing financial interest.

ACKNOWLEDGMENTS

REFERENCES

(1) (a) Johnson, N. B.; Lennon, I. C.; Moran, P. H.; Ramsden, J. A. *Acc. Chem. Res.* **2007**, *40*, 1291−1299. (b) Knowles, W. S.; Noyori, R. *Acc. Chem. Res.* **2007**, *40*, 1238−1239. (c) Saudan, L. A. *Acc. Chem. Res.* **2007**, *40*, 1309−1319.

(2) Mallat, T.; Orglmeister, E.; Baiker, A. *Chem. Rev.* **2007**, *107*, 4863−4890.

(3) (a) Zhang, W.; Chi, Y.; Zhang, X. *Acc. Chem. Res.* **2007**, *40*, 1278−1290. (b) Wang, D.-S.; Chen, Q.-A.; Lu, S.-M.; Zhou, Y.-G. *Chem. Rev.* **2012**, *112*, 2557−2590.

(4) Chirik, P.; Morris, R. *Acc. Chem. Res.* **2015**, *48*, 2495−2495.

(5) (a) Bart, S. C.; Lobkovsky, E.; Chirik, P. J. *J. Am. Chem. Soc.* **2004**, *126*, 13794−13807. (b) Casey, C. P.; Guan, H. *J. Am. Chem. Soc.* **2007**, *129*, 5816−5817. (c) Mikhailine, A.; Lough, A. J.; Morris, R. H. *J. Am. Chem. Soc.* **2009**, *131*, 1394−1395. (d) Nakazawa, H.; Itazaki, M., Fe−H Complexes in Catalysis. In *Iron Catalysis: Fundamentals and Applications*; Plietker, B., Ed.; Springer: Berlin, Heidelberg, 2011; pp 27−81. (e) Chakraborty, S.; Dai, H.; Bhattacharya, P.; Fairweather, N. T.; Gibson, M. S.; Krause, J. A.; Guan, H. *J. Am. Chem. Soc.* **2014**, *136*, 7869−7872. (f) Chakraborty, S.; Bhattacharya, P.; Dai, H.; Guan, H. *Acc. Chem. Res.* **2015**, *48*, 1995−2003. (g) Li, Y.-Y.; Yu, S.-L.; Shen, W.-Y.; Gao, J.-X. *Acc. Chem. Res.* **2015**, *48*, 2587−2598. (h) Morris, R. H. *Acc. Chem. Res.* **2015**, *48*, 1494−1502. (i) Stalzer, M. M.; Nicholas, C. P.; Bhattacharyya, A.; Motta, A.; Delferro, M.; Marks, T. J. *Angew. Chem., Int. Ed.* **2016**, *55*, 5263−5267.

(6) (a) Chen, F.; Surkus, A.-E.; He, L.; Pohl, M.-M.; Radnik, J.; Topf, C.; Junge, K.; Beller, M. *J. Am. Chem. Soc.* **2015**, *137*, 11718−11724. (b) Zhang, G.; Scott, B. L.; Hanson, S. K. *Angew. Chem., Int. Ed.* **2012**, *51*, 12102−12106.

(7) Bellow, J. A.; Yousif, M.; Cabelof, A. C.; Lord, R. L.; Groysman, S. *Organometallics* **2015**, *34*, 2917−2923.

(8) Crabtree, R. *Acc. Chem. Res.* **1979**, *12*, 331−337.

(9) (a) Zhang, X.; Geng, Y.; Han, B.; Ying, M.-Y.; Huang, M.-Y.; Jiang, Y.-Y. *Polym. Adv. Technol.* **2001**, *12*, 642−646. (b) Jagadeesh, R. V.; Surkus, A.-E.; Junge, H.; Pohl, M.-M.; Radnik, J.; Rabeah, J.; Huan, H.; Schünemann, V.; Brückner, A.; Beller, M. *Science* **2013**, *342*, 1073−1076.

(10) (a) Stein, M.; Wieland, J.; Steurer, P.; Tölle, F.; Mülhaupt, R.; Breit, B. *Adv. Synth. Catal.* **2011**, *353*, 523−527. (b) Welther, A.; Bauer, M.; Mayer, M.; Jacobi von Wangelin, A. *ChemCatChem* **2012**, *4*, 1088−1093. (c) Hudson, R.; Hamasaka, G.; Osako, T.; Yamada, Y. M. A.; Li, C.-J.; Uozumi, Y.; Moores, A. *Green Chem.* **2013**, *15*, 2141−2148. (d) Kelsen, V.; Wendt, B.; Werkmeister, S.; Junge, K.; Beller, M.; Chaudret, B. *Chem. Commun.* **2013**, *49*, 3416−3418. (e) Mokhov, V. M.; Popov, Y. V.; Nebykov, D. N. *Russ. J. Gen. Chem.* **2014**, *84*, 622−628.

(11) (a) Furukawa, H.; Cordova, K. E.; O'Keeffe, M.; Yaghi, O. M. *Science* **2013**, *641*, 1230444. (b) Wang, C.; Liu, D.; Lin, W. *J. Am. Chem. Soc.* **2013**, *135*, 13222−13234.

(12) (a) Henschel, A.; Gedrich, K.; Kraehnert, R.; Kaskel, S. *Chem. Commun.* **2008**, 4192−4194. (b) Hwang, Y. K.; Hong, D.-Y.; Chang, J.-S.; Jhung, S. H.; Seo, Y.-K.; Kim, J.; Vimont, A.; Daturi, M.; Serre, C.; Férey, G. *Angew. Chem., Int. Ed.* **2008**, *47*, 4144−4148. (c) Yoon, M.; Srirambalaji, R.; Kim, K. *Chem. Rev.* **2012**, *112*, 1196−1231. (d) Vermoortele, F.; Ameloot, R.; Vimont, A.; Serre, C.; De Vos, D. *Chem. Commun.* **2011**, *47*, 1521−1523. (e) Li, B.; Zhang, Y.; Ma, D.; Li, L.; Li, G.; Li, G.; Shi, Z.; Feng, S. *Chem. Commun.* **2012**, *48*, 6151−6153. (f) Park, J.; Li, J.-R.; Chen, Y.-P.; Yu, J.; Yakovenko, A. A.; Wang, Z. U.; Sun, L.-B.; Balbuena, P. B.; Zhou, H.-C. *Chem. Commun.* **2012**, *48*, 9995−9997. (g) Thimmaiah, M.; Li, P.; Regati, S.; Chen, B.; Zhao, J. C.-G. *Tetrahedron Lett.* **2012**, *53*, 4870−4872. (h) Gascon, J.; Corma, A.; Kapteijn, F.; Llabrés i Xamena, F. X. *ACS Catal.* **2014**, *4*, 361−378. (i) Genna, D. T.; Wong-Foy, A. G.; Matzger, A. J.; Sanford, M. S. *J. Am. Chem. Soc.* **2013**, *135*, 10586−10589. (j) Fei, H.; Shin, J.; Meng, Y. S.; Adelhardt, M.; Sutter, J.; Meyer, K.; Cohen, S. M. *J. Am. Chem. Soc.* **2014**, *136*, 4965−4973. (k) Manna, K.; Zhang, T.; Lin, W. *J. Am. Chem. Soc.* **2014**, *136*, 6566−6569. (l) Manna, K.; Zhang, T.; Carboni, M.; Abney, C. W.; Lin, W. *J. Am. Chem. Soc.* **2014**, *136*, 13182−13185. (m) Pullen, S.; Fei, H.; Orthaber, A.; Cohen, S. M.; Ott, S. *J. Am. Chem. Soc.* **2013**, *135*, 16997−17003. (n) Zhao, M.; Ou, S.; Wu, C.-D. *Acc. Chem. Res.*

2014, *47*, 1199−1207. (o) Sawano, T.; Ji, P.; McIsaac, A. R.; Lin, Z.; Abney, C. W.; Lin, W. *Chem. Sci.* **2015**, *6*, 7163−7168. (p) Gonzalez, M. I.; Bloch, E. D.; Mason, J. A.; Teat, S. J.; Long, J. R. *Inorg. Chem.* **2015**, *54*, 2995−3005. (q) Thacker, N. C.; Lin, Z.; Zhang, T.; Gilhula, J. C.; Abney, C. W.; Lin, W. *J. Am. Chem. Soc.* **2016**, *138*, 3501−3509. (r) Manna, K.; Ji, P.; Greene, F. X.; Lin, W. *J. Am. Chem. Soc.* **2016**, *138*, 7488−7491.

(13) (a) Manna, K.; Zhang, T.; Greene, F. X.; Lin, W. *J. Am. Chem. Soc.* **2015**, *137*, 2665−2673. (b) McGuirk, C. M.; Katz, M. J.; Stern, C. L.; Sarjeant, A. A.; Hupp, J. T.; Farha, O. K.; Mirkin, C. A. *J. Am. Chem. Soc.* **2015**, *137*, 919−925. (c) Sawano, T.; Thacker, N. C.; Lin, Z.; McIsaac, A. R.; Lin, W. *J. Am. Chem. Soc.* **2015**, *137*, 12241−12248. (d) Zhang, T.; Manna, K.; Lin, W. *J. Am. Chem. Soc.* **2016**, *138*, 3241−3249. (e) Metzger, E. D.; Brozek, C. K.; Comito, R. J.; Dincă, M. *ACS Cent. Sci.* **2016**, *2*, 148−153.

(14) (a) Peters, A. W.; Li, Z.; Farha, O. K.; Hupp, J. T. *ACS Nano* **2015**, *9*, 8484−8490. (b) Kung, C.-W.; Mondloch, J. E.; Wang, T. C.; Bury, W.; Hoffeditz, W.; Klahr, B. M.; Klet, R. C.; Pellin, M. J.; Farha, O. K.; Hupp, J. T. *ACS Appl. Mater. Interfaces* **2015**, *7*, 28223−28230. (c) Klet, R. C.; Wang, T. C.; Fernandez, L. E.; Truhlar, D. G.; Hupp, J. T.; Farha, O. K. *Chem. Mater.* **2016**, *28*, 1213−1219.

(15) Manna, K.; Ji, P.; Lin, Z.; Greene, F. X.; Urban, A.; Thacker, N. C.; Lin, W. *Nat. Commun.*, **2016**, *7*, 12610.

(16) During the final preparation of this manuscript, a paper by Zhang and coworkers reported a related Zr MOF, but their Zr_8-SBUs were formulated differently. See: Zhang, X.; Zhang, X.; Johnson, J. A.; Chen, Y.-S.; Zhang, J. *J. Am. Chem. Soc.* **2016**, *138*, 8380−8383.

(17) Pu, L. S.; Yamamoto, A.; Ikeda, S. *J. Am. Chem. Soc.* **1968**, *90*, 3896−3896.

(18) Bonrath, W.; Medlock, J.; Tschumi, J. Process for the manufacture of 3,7-dimethyl-1-octen-3-ol. U.S. Patent WO2012025559 A3, July 19, 2012.

(19) (a) Lagaditis, P. O.; Sues, P. E.; Sonnenberg, J. F.; Wan, K. Y.; Lough, A. J.; Morris, R. H. *J. Am. Chem. Soc.* **2014**, *136*, 1367−1380. (b) Langer, R.; Leitus, G.; Ben-David, Y.; Milstein, D. *Angew. Chem.* **2011**, *123*, 2168−2172. (c) Rösler, S.; Obenauf, J.; Kempe, R. *J. Am. Chem. Soc.* **2015**, *137*, 7998−8001.

(20) Xu, R.; Chakraborty, S.; Yuan, H.; Jones, W. D. *ACS Catal.* **2015**, *5*, 6350−6354.